 CMES, vol.3, no.6, pp.731-741, 2002

A Two-dimensional Finite Element Implementation of a Special Form of Gradient Elasticity

L. Teneketzis Tenek[1] **and E.C. Aifantis**[1,2,3]

Abstract: A two-dimensional finite element implementation of a special form of gradient elasticity is developed and a connection between classical and the proposed gradient elasticity theory is established. A higher-order constitutive equation is adopted which involves a gradient term of a special form; the higher-order term is precisely the second gradient of the lower-order term. A weak form of the equilibrium equations, based on the principle of virtual work, is formulated for the classical problem. The problem in hand, is solved by means of the finite element method in two steps. First, the displacement field of classical elasticity is computed. Then, the gradient equation is solved using the displacement field extracted from the solution of the classical problem. In concert with the natural-mode finite element method, sets of rigid-body and straining modes are assigned to plane triangular elements for the classical problem. All elemental matrices are integrated explicitly. The theory is applied to two tensile notch specimens including a relatively large and a smaller notch, respectively. Numerical results reveal that the gradient theory yields more closely spaced deformation bands and a stiffer structural response. Strains for both theories are computed. The higher strain concentrations are localized at the notch tip for both specimens while the difference in strain patterns as obtained from both theories are more pronounced for the specimen with the smaller notch. The effect of the specimen size on the structural response and the corresponding size effect is also assessed.

1 Introduction

The inability of classical elasticity and plasticity theories to model stress-strain behavior adequately at small scales, to model strain gradient effects that may be important in linear elastic materials that contain microstructures, and their inability to predict the size effect observed at the micron scale in ductile materials since their constitutive models posses no internal length parameters, provided the motivation for the development of gradient elasticity and plasticity theories (Tenek and Aifantis (2001), Fleck and Hutchinson (1993, 1997), Fleck et al. (1994), Gao et al., (1999), Arharya and Bassani (2000), Huang et al. (2000b), Shi et al. (2000), Hutchinson and Hwang (1999)). Several finite elements for general strain gradient plasticity exist. (Wei and Hutchinson (1997), Shu et al., (1999), Svendberg and Runesson (2000), Xikui and Cescotto (1996), Ramaswamy and Aravas (1998)). The present study introduces a two-dimensional finite element implementation of a special form of gradient elasticity.

The need for higher order gradients in the theory of deformation for softening solids and heterogeneous microstructures was first pointed out by Aifantis (1983-84-89) in relation to the problems of shear band thickness and persistent slip band spacing. The idea was further elaborated by Aifantis (1984-87-92) and by Triantafyllidis and Aifantis (1986), and in more detail in a series of papers dealing with localization and stability of deformation in metals and soils. As a result, a higher-order strain gradient theory has been proposed by Aifantis and co-workers to address the heterogeneity and pattern development in elastic deformation and plastic flow.

A simple approach to solve boundary-value problems in gradient elasticity was introduced by Ru and Aifantis (1993). In general, one has to solve a fourth-order partial differential equation subjected to appropriate boundary conditions. Of course, the solution of a 4^{th} order problem directly, using classical finite elements, is rather cumbersome. The recent developments in Meshless Local Petrov-Galerkin (MPLG) methods, which very easily lead to C1 or C2 type of interpolations, appear to be preferable in solving problems involving gradient-

[1] Laboratory of Mechanics and Materials, Polytechnic School Aristotle University of Thessaloniki, GR-54006, Thessaloniki, Greece
[2] Center for Mechanics of Materials and Instabilities Michigan Technological University, Houghton MI 49931, USA
[3] Corresponding Author

theories Atluri and Shen (2002), Kim and Atluri (2000), Atluri and Zhu. As pointed out by Ru and Aifantis (1993) the complexity of this task can be reduced when the original fourth-order problem is reduced into a second-order problem. Thus, a connection between the gradient and classical solutions are established. Henceforth, it turns out that the problem in hand can be solved in two stages. Firstly, the classical elasticity problem is formulated and solved and the classical displacement field is acquired. There follows the solution of the gradient second order problem which has the classical displacement vector as a right-hand side. The gradient parameter is introduced on the second stage.

In the present paper we attempt a finite element solution of the gradient elasticity boundary-value problem. The problem is solved in two stages. Firstly, the principle of virtual work is formed in classical elasticity which yields the classical displacement field. Then, the solution of the gradient equation is attempted using the displacement field extracted from the solution of the classical problem according to the Galerkin methodology. All elemental matrices are explicitly integrated.

2 Mathematical model

A higher-order strain gradient theory developed by Ru and Aifantis (1993) adopts a simple constitutive equation of the form

$$\boldsymbol{\sigma} = \lambda(\mathrm{tr}\,\boldsymbol{\varepsilon})\mathbf{I} + 2\mu\boldsymbol{\varepsilon} - \mathrm{c}\nabla^2\left[\lambda(\mathrm{tr}\,\boldsymbol{\varepsilon})\mathrm{I} + 2\mu\boldsymbol{\varepsilon}\right], \tag{1}$$

where $(\boldsymbol{\sigma}, \boldsymbol{\varepsilon})$ are the stress and strain, (λ, μ) the Lame constants, ∇^2 the Laplacian and c a constant gradient coefficient. On introducing (1) with $c \equiv 0$ into the equilibrium equations ($\mathrm{div}\boldsymbol{\sigma} = 0$), we obtain the following differential equation for the displacement vector $\mathbf{u}$ ($2\varepsilon = \nabla\mathbf{u} + [\nabla\mathbf{u}]^T$):

$$\mathbf{L}\mathbf{u}^0 = 0, \qquad \mathbf{L} \equiv \mu\nabla^2 + (\lambda+\mu)\mathrm{grad\,div}. \tag{2}$$

On introducing (1) with $c \neq 0$ into the equilibrium equations we arrive at

$$(1 - c\nabla^2)\mathbf{L}\mathbf{u} = 0. \tag{3}$$

In general, one has to solve the fourth-order partial differential equation (3) subjected to appropriate boundary conditions. However, due to the fact that the operators L and ∇^2commute, the original problem (3) is reduced into a second-order problem, namely (Ru and Aifantis (1993))

$$(1 - c\nabla^2)\mathbf{u} = \mathbf{u}^0, \tag{4}$$

Equation (4) establishes a connection between classical and gradient elasticity.

Now the expression of the stress in classical elasticity is

$$\boldsymbol{\sigma}^0 = \mathbf{H}\boldsymbol{\varepsilon}^0 = \mathbf{H}\mathbf{D}\mathbf{u}^0, \tag{5}$$

or by using (5)

$$\boldsymbol{\sigma}^0 = \mathbf{H}\boldsymbol{\varepsilon}^0 = \mathbf{H}\mathbf{D}\mathbf{u}^0 = \mathbf{H}\mathbf{D}(1 - c\nabla^2)\mathbf{u} = \boldsymbol{\sigma} \tag{6}$$

which implies that the stress field of classical elasticity in cartesian coordinates coincides with that of gradient elasticity.

3 Computational model

The problem in hand is solved in two steps. First, equation (2) is solved by adopting classical finite element procedures, and more specifically the natural-mode finite element method (Argyris and Tenek (1996), Tenek and Argyris (1997-98)). In so doing, the displacement vector $\mathbf{u}^o$ is estimated. The classical solution, is based on the principle of virtual work which reads (Tenek and Argyris (1998))

$$\int_V \boldsymbol{\sigma}^t\, \delta\boldsymbol{\varepsilon}\, dV = \int_S \mathbf{p}_S^t\, \delta\mathbf{u}^o\, dS + \int_V \mathbf{p}_V^t\, \delta\mathbf{u}^o\, dV + \mathbf{R}^t\, \delta\mathbf{u}^o + \mathbf{M}^t\, \delta\boldsymbol{\vartheta}, \tag{7}$$

where, $(\boldsymbol{\sigma}, \boldsymbol{\varepsilon})$ are the vectors of stress and strain respectively; ($\mathbf{p}_S$, $\mathbf{p}_V$) the applied surface and volume forces, respectively; (**R**, **M**) the concentrated nodal forces and

moments, respectively; and ($\mathbf{u}^o$, $\boldsymbol{\theta}$) the nodal displacement and rotations, respectively. Then, equation (7) is applied on an elemental basis, i.e. on a triangular finite element. In concert with the natural-mode finite element method, the structure is discretized with a set of triangular finite elements. The elements are assigned sets of rigid-body and straining modes. The later are equal to the number of total nodal degrees of freedom minus the number of rigid-body modes. In so doing, and by following classical finite element procedures, a linear system of equations is formed and the classical displacement field $\mathbf{u}^o$ is computed. We focus now on the solution of the gradient equation (4).

We seek the weak form of (4). Adopting the Galerkin methodology, we multiply (4) by a test function $\tilde{\mathbf{u}}$ and integrate over a volume V, viz.

$$\int_V \mathbf{u}\tilde{\mathbf{u}}\, dV - \int_V c\nabla^2\mathbf{u}\tilde{\mathbf{u}}\, dV = \int_V \mathbf{u}^o\tilde{\mathbf{u}}\, dV. \tag{8}$$

Integrating the second term by parts

$$\int_V \mathbf{u}\,\tilde{\mathbf{u}}\, dV - \int_S c\,\nabla\mathbf{u}\tilde{\mathbf{u}}\, dS + \int_V c\,\nabla\mathbf{u}\,\nabla\tilde{\mathbf{u}}\, dV = \int_V \mathbf{u}^o\tilde{\mathbf{u}}\, dV, \tag{9}$$

where S denotes the surface (boundary) of the domain. Equation (9) will now be solved in two-dimensions x, y, for displacements u, v. Expanding terms in (9)

$$\int_V \mathrm{u}\,\tilde{\mathrm{u}}\, dV + c\int_V \left[\frac{\partial \mathrm{u}}{\partial \mathrm{x}}\frac{\partial \tilde{\mathrm{u}}}{\partial \mathrm{x}} + \frac{\partial \mathrm{u}}{\partial \mathrm{y}}\frac{\partial \tilde{\mathrm{u}}}{\partial \mathrm{y}}\right] dV - c\int_S \left(\frac{\partial \mathrm{u}}{\partial \mathrm{x}}n_1 + \frac{\partial \mathrm{u}}{\partial \mathrm{y}}n_2\right)\tilde{\mathrm{u}}\,\mathrm{dS} = \int_V \mathrm{u}^o\tilde{\mathrm{u}}\, dV, \tag{10}$$

$$\int_V \mathrm{v}\,\tilde{\mathrm{v}}\, dV + c\int_V \left[\frac{\partial \mathrm{v}}{\partial \mathrm{x}}\frac{\partial \tilde{\mathrm{v}}}{\partial \mathrm{x}} + \frac{\partial \mathrm{v}}{\partial \mathrm{y}}\frac{\partial \tilde{\mathrm{v}}}{\partial \mathrm{y}}\right] dV - c\int_S \left(\frac{\partial \mathrm{v}}{\partial \mathrm{x}}n_1 + \frac{\partial \mathrm{v}}{\partial \mathrm{y}}n_2\right)\tilde{\mathrm{v}}\,\mathrm{dS} = \int_V \mathrm{v}^o\tilde{\mathrm{v}}\, dV. \tag{11}$$

In equations (10), (11), n_1, n_2 are components of the unit vector outward to the surface S in the x and y directions, respectively. The above equations represent two uncoupled integral equations in x and y. We seek now a finite element solution of (10), (11). We will focus solely on (10). Equation(11) yields similar elemental matrices.

We consider a three-node triangular element with vertices 1,2,3, and a local cartesian coordinate system x', y' placed at the element barycenter. Usually, coordinate x' is considered parallel to edge 23. We shall use the triangular homogeneous coordinates $\zeta_1\zeta_2\zeta_3$ for which it holds (Tenek and Argyris (1998))

$$\varsigma_1 + \varsigma_2 + \varsigma_3 = 0. \tag{12}$$

Then, the displacement and test functions are interpolated from the nodal displacements u_1, u_2, u_3 via

$$u = u_1\varsigma_1 + u_2\varsigma_2 + u_3\varsigma_3, \qquad \tilde{u} = \tilde{u}_1\varsigma_1 + \tilde{u}_2\varsigma_2 + \tilde{u}_3\varsigma_3. \tag{13}$$

For the derivatives

$$\begin{aligned} \frac{\partial u}{\partial x} &= u_1\frac{\partial \varsigma_1}{\partial x} + u_2\frac{\partial \varsigma_2}{\partial x} + u_3\frac{\partial \varsigma_3}{\partial x}, \\ \frac{\partial u}{\partial y} &= u_1\frac{\partial \varsigma_1}{\partial y} + u_2\frac{\partial \varsigma_2}{\partial y} + u_3\frac{\partial \varsigma_3}{\partial y} \end{aligned} \quad . \tag{14}$$

In the above, all derivatives are referred to a global common cartesian coordinate x, y. We aim at deriving explicitly integrated elemental matrices and to this purpose we bring in the local cartesian coordinates x', y'. Explicitly for x

$$\frac{\partial u}{\partial x} = u_1\frac{\partial \varsigma_1}{\partial x'}\frac{\partial x'}{\partial x} + u_2\frac{\partial \varsigma_2}{\partial x'}\frac{\partial x'}{\partial x} + u_3\frac{\partial \varsigma_3}{\partial x'}\frac{\partial x'}{\partial x} \quad . \tag{15}$$

But

$$\frac{\partial x'}{\partial x} = c_{x'x}, \frac{\partial y'}{\partial y} = c_{y'y}, \tag{16}$$

where $c_{x'x}$, $c_{y'y}$ are the direction cosines of the local elemental axes with respect to the global axes, respectively. On account of (16), equation (15) becomes

$$\begin{aligned}\frac{\partial u}{\partial x} &= u_1\frac{\partial \varsigma_1}{\partial x'}c_{x'x}+u_2\frac{\partial \varsigma_2}{\partial x'}c_{x'x}+u_3\frac{\partial \varsigma_3}{\partial x'}c_{x'x},\\ \frac{\partial u}{\partial y} &= u_1\frac{\partial \varsigma_1}{\partial y'}c_{y'y}+u_2\frac{\partial \varsigma_2}{\partial y'}c_{y'y}+u_3\frac{\partial \varsigma_3}{\partial y'}c_{y'y}\end{aligned}. \tag{17}$$

For a triangle (Tenek and Argyris (1998))

$$\begin{aligned}&\frac{\partial \varsigma_1}{\partial x'}=-\frac{y_\alpha}{2\,\Omega},\quad \frac{\partial \varsigma_2}{\partial x'}=-\frac{y_\beta}{2\,\Omega},\quad \frac{\partial \varsigma_3}{\partial x'}=-\frac{y_\gamma}{2\,\Omega},\\ &\frac{\partial \varsigma_1}{\partial y'}=\frac{x_\alpha}{2\,\Omega},\quad \frac{\partial \varsigma_2}{\partial y'}=\frac{x_\beta}{2\,\Omega},\quad \frac{\partial \varsigma_3}{\partial y'}=-\frac{x_\gamma}{2\,\Omega},\end{aligned} \tag{18}$$

with

$$\begin{aligned}&x_\alpha=x_{23}=x_3-x_2,\quad x_\beta=x_{31}=x_1-x_3,\\ &y_\alpha=y_{23}=y_3-y_2,\quad y_\beta=y_{31}=y_1-y_3,\\ &x_\gamma=x_{12}=x_2-x_1,\quad y_\gamma=y_{12}=y_2-y_1,\end{aligned} \tag{19}$$

$$\Omega=\tfrac{1}{2}\begin{bmatrix}x_1 & y_1 & 1\\ x_2 & y_2 & 1\\ x_3 & y_3 & 1\end{bmatrix}$$

where Ω is the area of the triangle in terms of nodal coordinates. On account of (18), equation (17) now reads

$$\begin{aligned}\frac{\partial u}{\partial x} &= -c_{x'x}\left(\frac{y_\alpha}{2\,\Omega}u_1+\frac{y_\beta}{2\,\Omega}u_2+\frac{y_\gamma}{2\,\Omega}u_3\right),\\ \frac{\partial u}{\partial y} &= c_{y'y}\left(\frac{x_\alpha}{2\,\Omega}u_1+\frac{x_\beta}{2\,\Omega}u_2+\frac{x_\gamma}{2\,\Omega}u_3\right)\end{aligned}. \tag{20}$$

Substituting (13), (20) in equation (10) and using the integration formula

$$\frac{1}{\Omega}\int_\Omega \zeta_1^p\zeta_1^q\zeta_1^r d\Omega=\frac{2!p!q!r!}{(2+p+q+r)!}, \tag{21}$$

we derive an explicitly integrated finite element matrix based on (10). Proceeding in this manner, equations (10), (11) yield the elemental matrix

$$T=\Omega\begin{bmatrix}m_{11} & . & m_{12} & . & m_{13} & .\\ & m_{11} & . & m_{12} & . & m_{13}\\ & & m_{22} & . & m_{23} & .\\ & & & m_{22} & . & m_{23}\\ & Symm. & & & m_{33} & .\\ & & & & & m_{33}\end{bmatrix}. \tag{22}$$

The entries of matrix **T** read as follow:

$$\begin{aligned}m_{11} &= \frac{1}{6}+c\left(\frac{1}{4}\frac{c_{x'x}^2y_\alpha^2}{\Omega^2}+\frac{1}{4}\frac{c_{y'y}^2x_\alpha^2}{\Omega^2}\right),\\ m_{12} &= \frac{1}{12}+c\left(\frac{1}{4}\frac{c_{x'x}^2y_\beta y_\alpha}{\Omega^2}+\frac{1}{4}\frac{c_{y'y}^2x_\beta x_\alpha}{\Omega^2}\right),\\ m_{13} &= \frac{1}{12}+c\left(\frac{1}{4}\frac{c_{x'x}^2y_\gamma y_\alpha}{\Omega^2}+\frac{1}{4}\frac{c_{y'y}^2x_\gamma x_\alpha}{\Omega^2}\right),\\ m_{22} &= \frac{1}{6}+c\left(\frac{1}{4}\frac{c_{x'x}^2y_\beta^2}{\Omega^2}+\frac{1}{4}\frac{c_{y'y}^2x_\beta^2}{\Omega^2}\right),\\ m_{23=} &\frac{1}{12}+c\left(\frac{1}{4}\frac{c_{x'x}^2y_\gamma y_\beta}{\Omega^2}+\frac{1}{4}\frac{c_{y'y}^2x_\gamma x_\beta}{\Omega^2}\right),\\ m_{33} &= \frac{1}{6}+c\left(\frac{1}{4}\frac{c_{x'x}^2y_\gamma^2}{\Omega^2}+\frac{1}{4}\frac{c_{y'y}^2x_\gamma^2}{\Omega^2}\right).\end{aligned} \tag{23}$$

We are left to estimate the right-hand side of (10), (11). Proceeding in a similar manner, we obtain

$$\mathbf{R}=\Omega\begin{bmatrix}\frac{1}{6}u_1^o+\frac{1}{12}u_2^o+\frac{1}{12}u_3^o\\ \frac{1}{6}v_1^o+\frac{1}{12}v_2^o+\frac{1}{12}v_3^o\\ \frac{1}{12}u_1^o+\frac{1}{6}u_2^o+\frac{1}{12}u_3^o\\ \frac{1}{12}v_1^o+\frac{1}{6}v_2^o+\frac{1}{12}v_3^o\\ \frac{1}{12}u_1^o+\frac{1}{12}u_2^o+\frac{1}{6}u_3^o\\ \frac{1}{12}v_1^o+\frac{1}{12}v_2^o+\frac{1}{6}v_3^o\end{bmatrix}. \tag{24}$$

Following computation of the elemental matrix and vector, standard finite element procedures are adopted that

result in the estimation of structural deformation. After the nodal displacements are computed, the strains, assigned to the element center, are estimated using (20) and the definitions

$$\varepsilon_{xx} = \frac{\partial u}{\partial x}, \quad \varepsilon_{yy} = \frac{\partial v}{\partial y}, \quad \gamma_{xy} = \frac{\partial u}{\partial y} + \frac{\partial v}{\partial x}. \tag{25}$$

4 Computational experiments

Figure 1 shows a two-dimensional tensile notch specimen with material and geometrical data. Due to symmetry, one-quarter of the specimen is discretized with triangular elements and appropriate boundary conditions are imposed. The gradient coefficient is equal to c=5x10^{-5} m^2. On top of figure 2 is displayed the finite element mesh including 128 nodes and 215 elements. The structural deformation as obtained by the solution of the classical problem is illustrated in the middle of figure 2, while the displacement field resulted from the gradient model is presented on the bottom of the same figure. Figure 3 shows contours of the horizontal displacements from the solution of the classical problem and figure 4 horizontal displacement contours obtained by the solution of the gradient equation. We observe that the gradient solution yields more closely spaced deformation bands. Figures 5, 6 illustrate the vertical displacement field v. We observe that on the top specimen boundary the gradient solution yields an noticeable edge effect.

Horizontal displacements across sections A-A, and B-B for both theories are given in figures 7, 8. Close to the notch, the gradient theory yields a stiffer response (figure 7), while close to the middle of the specimen and away from the loaded edge the two theories yield close values (figure 8).

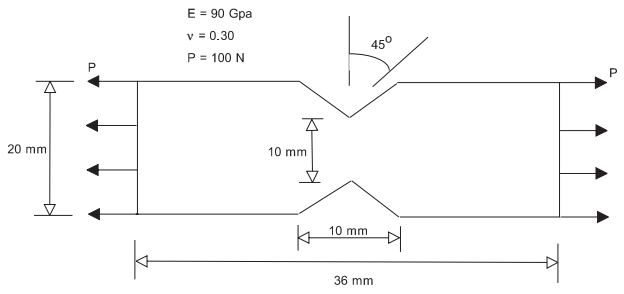

Figure 1 : Tensile notch specimen

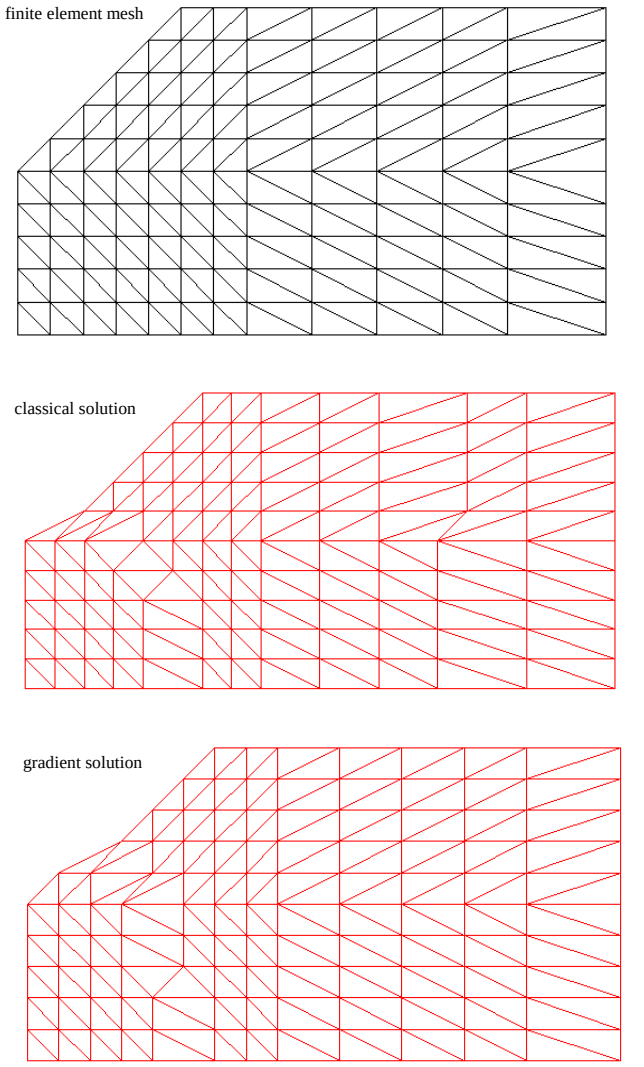

Figure 2 : Finite element mesh of quarter specimen (top); deformation as obtained by classical solution (middle); deformation as obtained by gradient solution (bottom)

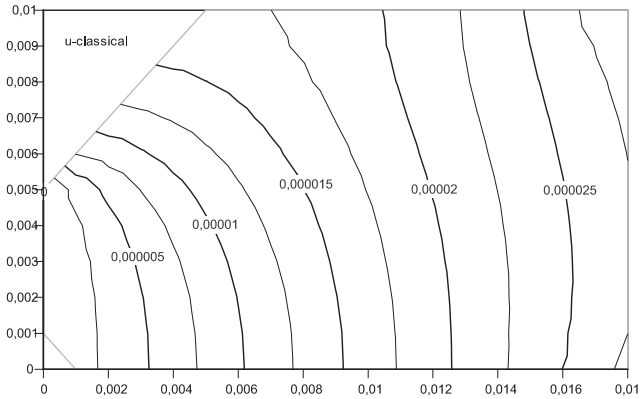

Figure 3 : Classical horizontal displacement contours

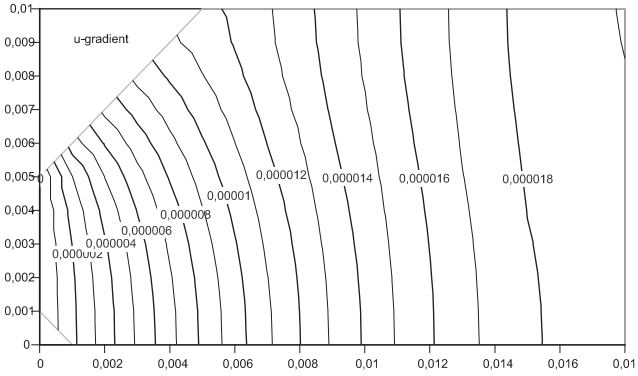

Figure 4 : Gradient horizontal displacement contours

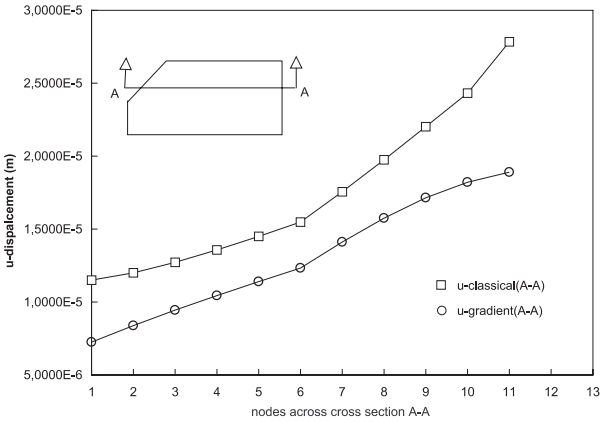

Figure 7 : Horizontal displacements across section A-A

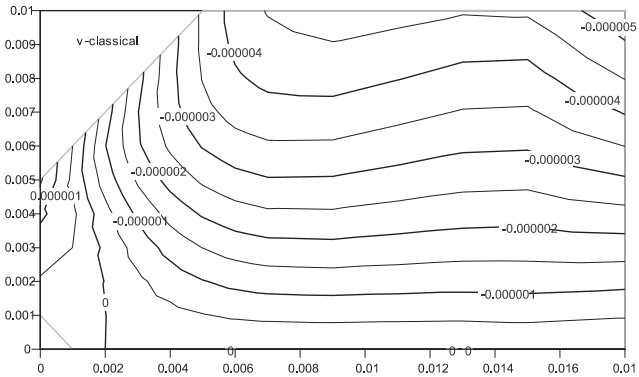

Figure 5 : Classical vertical displacement contours

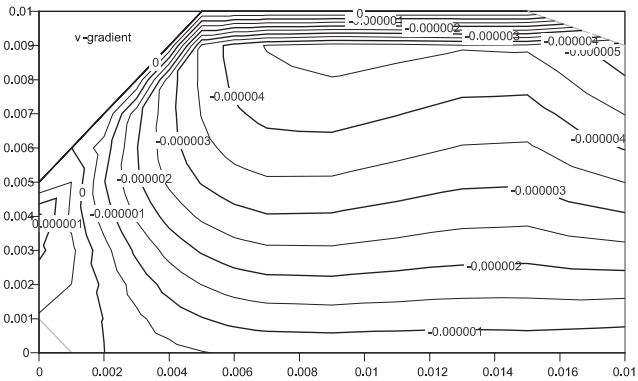

Figure 6 : Gradient vertical displacement contours

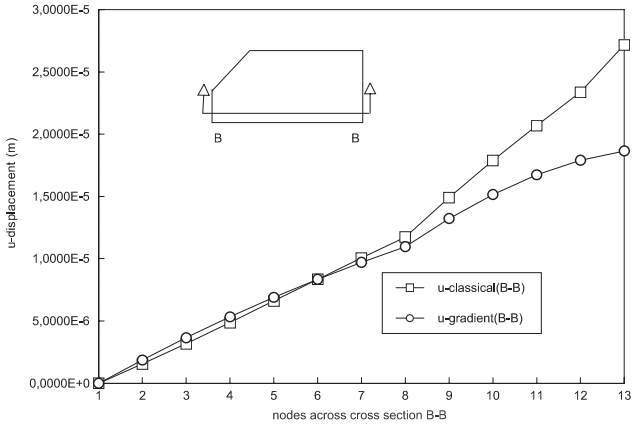

Figure 8 : Horizontal displacements across section B-B

As we approach the right edge, the gradient solution gives a stiffer response. Figure 9 shows the horizontal strains as computed with classical elasticity. The higher strains are localized at the notch tip. A similar picture is obtained for the gradient strains, however the later are more concentrated on vertical bands as figure 10 indicates. Vertical strain contours are provided in figures 11 and 12. Again, the gradient strains are spread in more bands and in addition, high strains appear on the top specimen boundary in contrary to the classical strains which show on the left boundary and the notch edge. The classical and gradient shear strains are displayed in figures 13 and 14. They are both concentrated around the notch tip, however the gradient shear strains are more localized. Finally, the effect of the specimen size on the structural response is assessed. To this purpose, three specimens with quarter bottom sides a=2mm, 18mm and 100mm are considered and the classical and gradient deformation and strain fields are obtained.

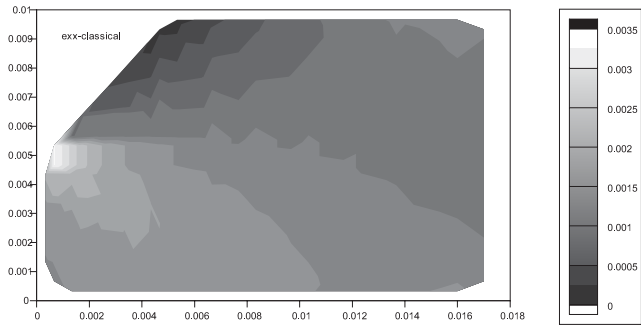

Figure 9 : Contours of classical axial strain

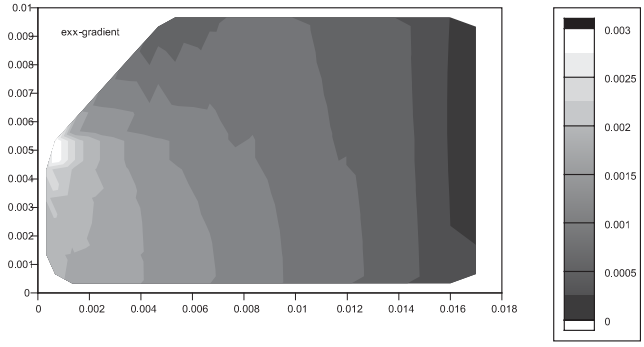

Figure 10 : Contours of gradient axial strain

Figure 15 displays the horizontal displacement of point 3 (bottom-right corner) for all specimens for both the classical and gradient cases. As expected, the classical theory

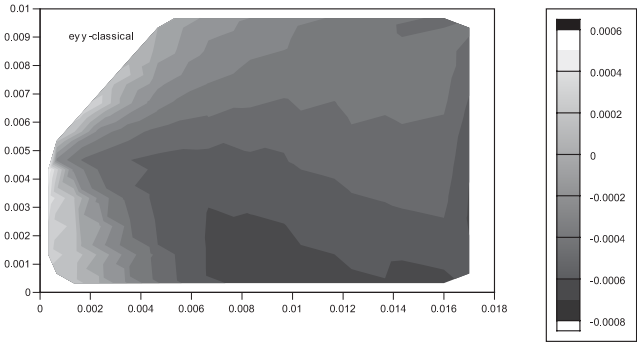

Figure 11 : Contours of classical vertical strain

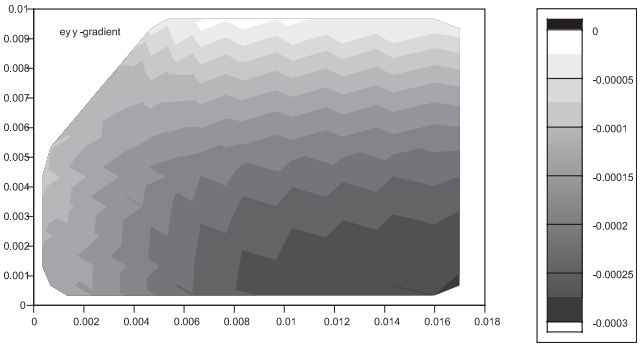

Figure 12 : Contours of gradient vertical strain

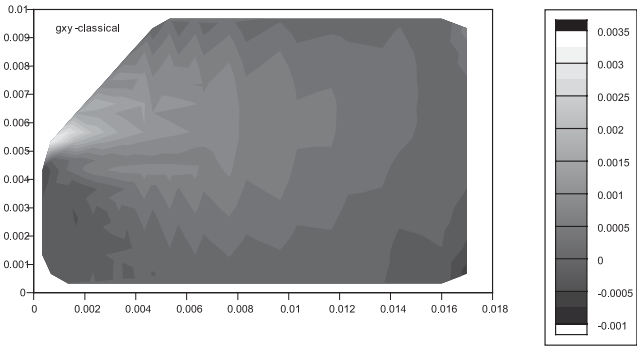

Figure 13 : Contours of classical shear strain

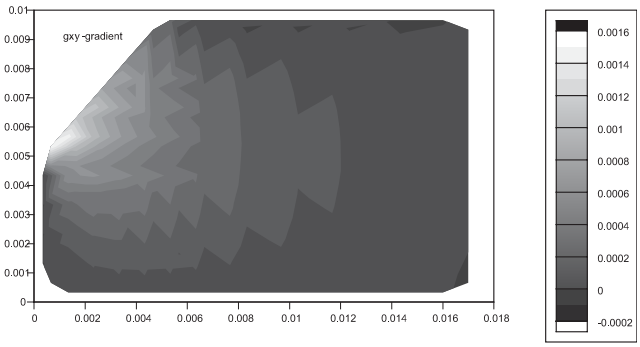

Figure 14 : Contours of gradient shear strain

results are independent of the specimen size. However, gradient theory predicts different displacements for the three specimens. Notably, the smaller the specimen, the stiffer the response. We also observe from figure 15 that as the size of the specimen increases the gradient solution approaches the classical solution. Figure 16 presents stress-strain plots for all aforementioned specimen sizes. The size effect can be clearly discerned from the plot. Notably, for a specified displacement, the specimen with side 2mm requires a larger force than the specimens with sides 18 and 100 mm, respectively. The specimen with side equal to 18mm (and all other specimen dimensions increased proportionally) requires a larger force than the specimen with size 100mm. Thus, the size effect can be distinguished from figure 16.

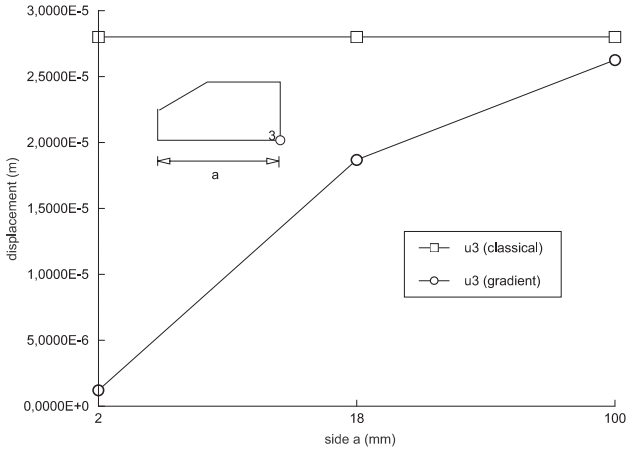

Figure 15 : Horizontal displacement of point 3 with specimen size

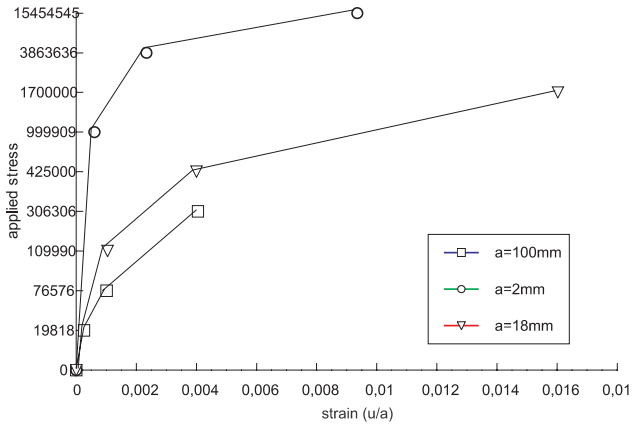

Figure 16 : Size effect for tensile notch specimen

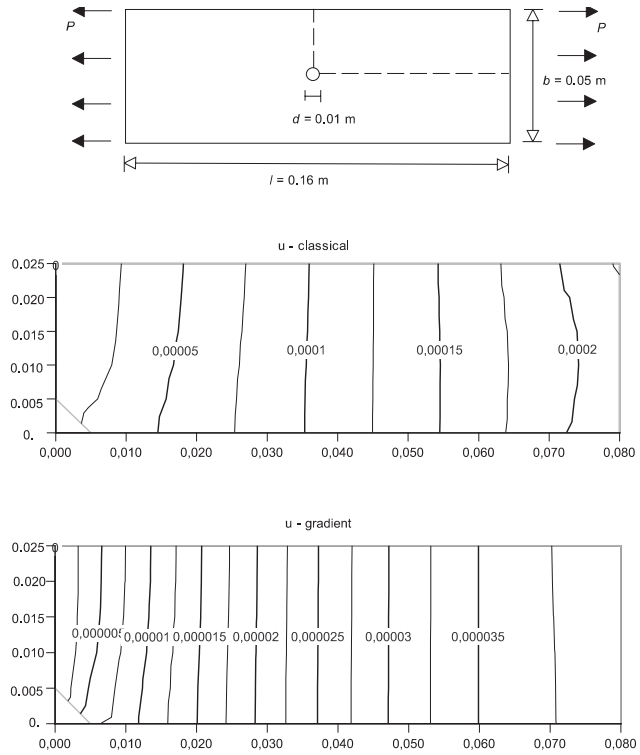

Figure 17 : Tensile specimen with a central notch; horizontal displacement fields

We consider next a tensile specimen with a central notch shown in Fig. 17. The side of the specimen is 16 times larger than the diameter of the notch. Again, a quarter of the specimen is discretized with a set of plane triangular elements and symmetry boundary conditions are imposed so that the left edge cannot move horizontally (u=0) and the bottom edge cannot move vertically (v=0). All material parameters are kept the same as for the previous problem of Fig. 1. The resulting horizontal displacement fields as given by classical and gradient deformation theories are plotted in the middle and bottom of Fig. 17, respectively. We observe that gradient theory, as for the previous problem, yields more closely spaced deformation bands and also yields a stiffer structural response. Figure 18 presents the horizontal strain fields for both classical (top) and gradient (bottom) models. For both models, high strain localization occurs near the central notch and higher strain appears for the classical model. The latter, predicts strain patterns that emanate from the notch and propagate throughout the specimen. On the contrary, for gradient theory horizontal strains are localized at the notch area while at the rest of the specimen vertical strain bands and patterns are dominant. Thus,

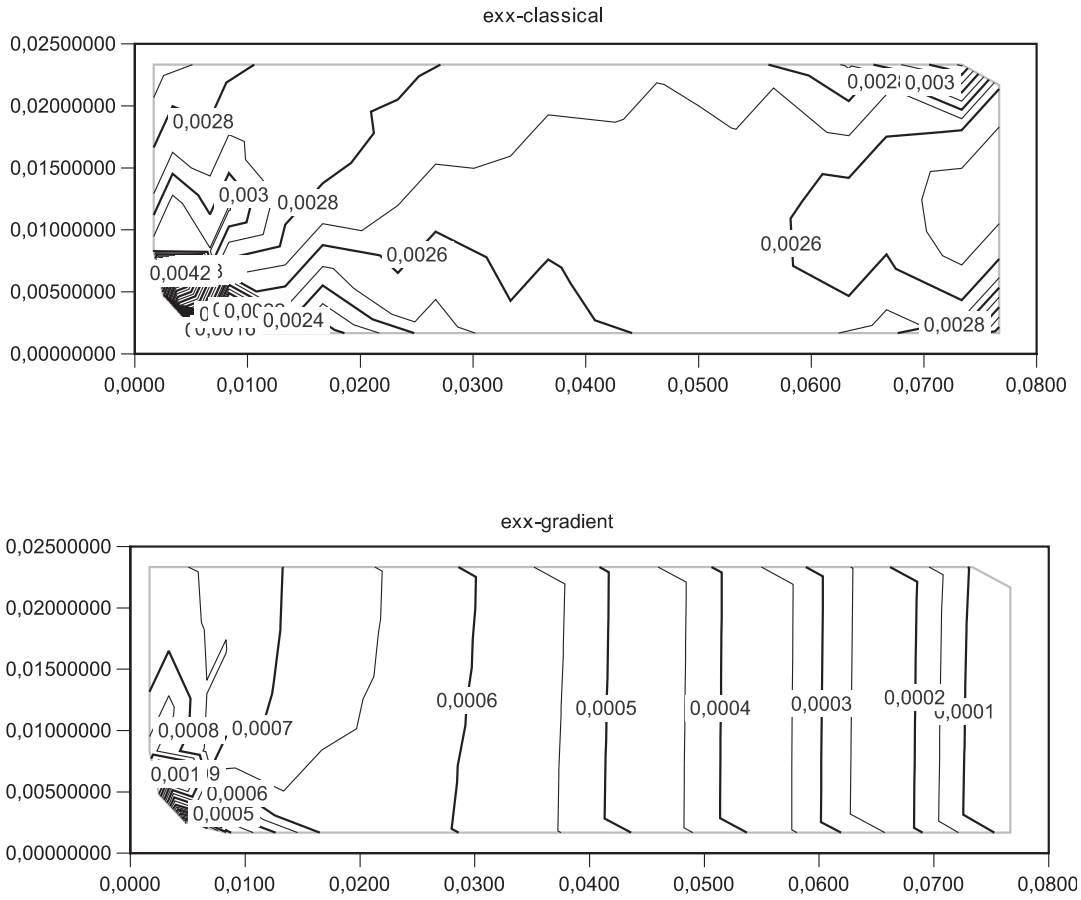

Figure 18 : Classical and gradient horizontal strains

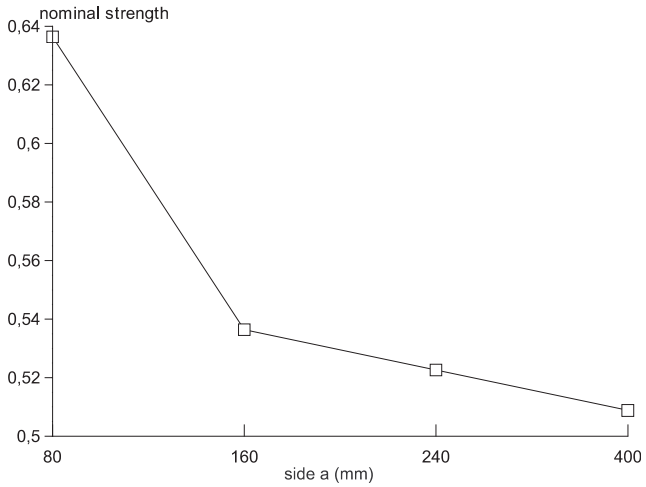

Figure 19 : Size effect for the tensile notch specimen

the pattern field of the horizontal strains appears different for the classical elasticity and the gradient elasticity theories, respectively. Figure 19 displays the size effect for the notch specimen of Fig.17. To this purpose, all dimensions are increased proportionally, and the nominal strength versus specimen side are plotted. It is evident that the smaller specimen displays the higher nominal strength.

5 Conclusions

A two-dimensional finite element implementation of a special form of gradient elasticity is developed. A higher-order constitutive equation is adopted which involves a gradient term of a special form; the higher-order term is precisely the second gradient of the lower-order term. A weak form of the equilibrium equations, based on the principle of virtual work, is formulated for the classical problem. The problem in hand, is solved by means of the finite element method. The limitation of the nu-

merical procedure lies in the special constitutive relation adopted and the fact that the stress field remains the same for both classical and gradient elasticity theories. Two tensile notch specimens are considered which implement the theory. For both test problems the size effect is computed.

Acknowledgement: The financial support of the Greek general secretariat of research and technology under grant PENED 99-1958 is gratefully acknowledged

References

Acharya, A., Bassani, J.L. (2000): Lattice incompatibility and a gradient theory of crystal plasticity, *J. Mech. Phys. Solids*, 48, pp. 1565-1595

Aifantis, E.C. (1989): Some thoughts on degrading materials, in NSF Workshop on Mechanics of Damage and Fracture, (eds. S.N. Atluri and J.E. Fitzgerald), Georgia Tech., Atlanta, GA, pp 1-12

Aifantis, E.C. (1983): Dislocation kinetics and the formation of deformation bands, in Defects, Fracture and Fatigue, (eds. G.C. Sih and J.W. Provan), Martinus-Nijhoff, The Hague, pp 75-84

Aifantis, E.C. (1984): On the mechanics of modulated structures, in Modulated Structure Materials, NATO ASI Series 83 (ed. T. Tsakalakos), Martinus-Nijhoff, Dordrecht, pp. 357-385

Aifantis, E.C. (1984): On the microstructural origin of certain inelastic models., *J. Mat. Engng. Tech.*, Vol. 106, pp. 326-330

Aifantis, E.C. (1987): The physics of plastic deformation, *Int. J. Plasticity*, Vol. 3, pp. 211-247

Aifantis, E.C. (1992): On the role of gradients in the localization of deformation and fracture, *Int. J. Engng. Sci.*, Vol. 30, pp. 1279-1299

Argyris, J., Tenek, L. (1996): Natural mode method: A practicable and novel approach to the global analysis of laminated composite plates and shells, *Applied Mechanics Reviews*, Volume 49(5), July 1996, pp. 381-389

Atluri, SN & Shen, S (2002): *The Meshless Local Petrov-Galerkin (MPLG) Method*, Tech Science Press, 430 pages

Atluri, Sn & Shen, S (2002): The meshless Local Petrov-Galerkin (MLPG) Method: A Simple & Less-Costly Alternative to the Finite Element and Boundary Element Methods, *CMES: Computer Modeling in Engineering & Sciences*, Vol. 3, No. 1, pp. 11-52

Atluri, SN., and Zhu, T. (1998): A New Meshless Local Petrov-Galerkin (MLPG) Approach in Computational Mechanics, Vol.22, pp. 117-127.

Fleck, N.A. Hutchinson J.W. (1993): A phenomenological theory for strain gradient effects in plasticity, 41, *J. Mech. Phys. Solids*, pp. 1825-1857

Fleck, N.A. Hutchinson J.W. (1997): Strain gradient plasticity. In: Hutchinson, J.W., Wu, T.Y. (Eds.), *Advances in Applied Mechanics*, 33, Academic Press, New York, pp. 295-361

Fleck, N.A., Muller, G.M., Ashby, M.F., Hutchinson, J.W. (1994): Strain gradient plasticity: theory and experiments, *Acta Mettal. Mater.*, 42, pp. 475-487

Gao, H., Huang, Y., Nix, W.D., Hutchinson, J.W. (1999): Mechanism-based strain gradient plasticity-I. Theory, *J. Mech. Phys. Solids*, 47, pp. 1239-1263

Huang, Y., Gao, H., Nix, W.D., Hutchinson, J.W. (2000b): Mechanism-based strain gradient plasticity-II. Analysis, *J. Mech. Phys. Solids*, 48, pp. 99-128

Hutchinson, J.W., Hwang, K.C. (1999): The crack tip fields in strain gradient plasticity: the asymptotic and numerical analyses, *Eng. Fracture Mechanics*, 64(5), pp. 625-648

Kim, H.G.; Atluri, S.N. (2000): Arbitrary Placement of Secondary Nodes, and Error Control, in the Meshless Local Petrov-Galerkin (MLPG) Method, *CMES: Computer Modeling in Engineering & Sciences*, Vol. 1, No. 3, pp. 11-32

Ramaswamy, S., Aravas., N. (1998): Finite element implementation of gradient plasticity models Part I: Gradient-dependent yield functions, *Comput. Meth. Appl. Mech. Eng.*, 163(1-4), pp. 11-32

Ramaswamy, S., Aravas., N. (1998): Finite element implementation of gradient plasticity models Part II: Gradient-dependent evolution equations, *Comput. Meth. Appl. Mech. Eng.*, 163(1-4), pp. 33-53

Ru, C. Q., Aifantis, E. C. (1993): A simple approach to solve boundary-value problems in gradient elasticity, *Acta Mechanica 101*, pp. 59-68

Shi, M.X., Huang, Y., Hwang, K.C. (2000): Fracture in a higher-order elastic continuum, *J. Mech.. Phys. Solids*, 48, pp. 2513-2538

Shu, J.Y., King, W.E., Fleck, N.A. (1999): Finite ele-

ments for materials with strain gradient effects, *Int. J. Numer. Meth. Engng.*, 44, pp. 373-391

Svendberg, T., Runesson, K. (2000): An adaptive finite element algorithm for gradient theory of plasticity with coupling to damage, *Int. J. Solids and Structures*, 37(48-50), pp. 7481-7499

Tenek, L.T., Aifantis, E.C. (2001): On some applications of gradient elasticity to composite materials, *Composite Structures*, 53, pp. 189-197

Tenek, L., Argyris, J. (1997): Computational aspects of the natural-mode finite element method, *Commun. Numer. Methods Eng.*, 13, pp. 705-713

Tenek, L., Argyris, J. (1998): *Finite element analysis for composite structures*, Kluwer Academic Publishers, Dordrecht, The Netherlands

Triantafyllidis, N., Aifantis, E. C. (1986): A gradient approach to localization of deformation-I. Hyperelastic materials, *J. Elasticity*, 16, pp. 225-238

Xikui, L., Cescotto, S. (1996): Finite element method for gradient plasticity at large strains, *Int. J. Rock Mech. And Minimg Sci. & Geomechanics Abstracts*, 33, p. 301A

Wei., Y., Hutchinson, J.W. (1997): Steady-state crack growth and work of fracture for solids characterized by strain gradient plasticity, *J. Mech. Phys. Solids*, 45, pp. 1253-1273